# Magnetic Levitational Assembly for Living Material Fabrication

*Savas Tasoglu,* Chu Hsiang Yu, Volha Liaudanskaya, Sinan Guven, Claudio Migliaresi, and Utkan Demirci**

Assembly with guidance of field forces or without guidance is a promising and noninvasive strategy for aligning and biomanufacturing soft biological systems made of numerous heterogeneous microcomponents.[1,2] Several self-assembly strategies employing principles such as fluidic force,[3] surface energy,[4] magnetic force,[5,6] gravity,[7] electrostatic force, or capillary force[8,9] have been developed for many applications in optoelectronics, microfabrication, sensors, and tissue engineering.[1,8,10] Recently, hybrid approaches so-called "guided self-assembly" using railed microfluidics,[11] magnetics,[6,12,13] and acoustics[14] have been developed. These assembly methods are often massively parallel, and thus, less expensive and faster, which makes them convenient for complex soft material fabrication compared to deterministic approaches.

Microstructure patterning and assembly strategies using permanent magnets for advanced manufacturing are versatile, contact-free, and inexpensive.[15] Paramagnetic manipulation by magnetizing soft or hard objects of interest via magnetic micro/nanobeads and guiding their motion with magnetic field has been extensively studied in several applications such as bottom-up tissue engineering, diagnostics, and complex soft material fabrication.[6,13,16] Several applications of manipulation of objects in a paramagnetic salt solution have been demonstrated such as for detection of fat content in food samples,[17] to measure densities of solids and liquids,[18] to study binding of protein to gel-immobilized ligands,[19] and most recently to study noncontact orientation of objects in 3D.[20] Earlier work on manipulation of objects in ferrofluids was demonstrated to study collective behavior of polystyrene beads.[21] Detection of nonmagnetic bioparticles inside ferrofluids has been also studied.[22] More recently, assembly patterns using two-particle and three-particle systems (with one magnetic and one or two nonmagnetic beads, respectively) have been studied in ferrofluids.[23] A microseparation and sorting platform with no external flow creating locally programmable magnetic fields and manipulating cells based on size, shape, and elasticity has been also shown.[24] More recently, a flow-through manipulation and separation of microparticles using ferrofluids has been demonstrated by the same group.[25] However, diamagnetic manipulation by magnetizing the suspending media of target objects and guiding their assembly towards a magnetic minima has not been studied for soft living material fabrication which has a broad range of applications, including bottom-up tissue engineering and microphysiological system engineering. Compared to use of magnetic beads made of mainly iron oxide with minimal amounts of other elements such as nickel and cobalt, encapsulated in a polymer shell, in levitation approaches, mostly ions such as gadolinium ($Gd^{3+}$) and manganese ($Mn^{2+}$) or radicals have been used to paramagnetize suspending media.[6,13,15] High concentrations of $Gd^{3+}$ salts can be unhealthy for cells. There are paramagnetic Gd formulations that are clinically used for magnetic resonance imaging (MRI) investigations in humans.[26] For life science applications, there is a risk of osmotic pressure imbalance due to excessive use of ions in levitation approaches as opposed to a risk of toxicity in the case of using magnetic particles for paramagnetic manipulation approaches. This limitation can be addressed by either or combination of stronger magnetic fields and smaller density differences between building blocks and suspending media. With the remote manipulation capability, levitational diamagnetic assembly strategy can provide a powerful tool to manipulate and assemble soft small living blocks to create complex microenvironments for tissue engineering, and/or micromanufacturing of soft systems.

Here, we present a powerful, yet, simple approach to create living soft materials using a levitation-based magnetic method. This strategy allowed the alignment of microstructures such

Prof. S. Tasoglu, C. H. Yu
Department of Mechanical Engineering
University of Connecticut
191 Auditorium Road, Storrs, CT 06269, USA
E-mail: savas@engr.uconn.edu
Prof. S. Tasoglu
Department of Biomedical Engineering
University of Connecticut
260 Glenbrook Road, Storrs, CT 06269, USA
C. H. Yu, Prof. U. Demirci
Center for Bioengineering
Brigham and Women's Hospital
Harvard Medical School
Boston, MA 02115, USA
V. Liaudanskaya, Dr. C. Migliaresi
European Institute of Excellence on Tissue Engineering and Regenerative Medicine
Trento, 38123 Italy
V. Liaudanskaya, Dr. C. Migliaresi
Department of Industrial Engineering
Biotech Research Center
University of Trento
Via Sommarive 9, 38123 Trento, Italy
V. Liaudanskaya, S. Guven, Prof. U. Demirci
Bio-Acoustic MEMS in Medicine (BAMM) Laboratory
Canary Center at Stanford for Cancer Early Detection
Department of Radiology
Stanford School of Medicine
Palo Alto, CA 94304, USA
E-mail: utkan@stanford.edu

**DOI: 10.1002/adhm.201500092**

  

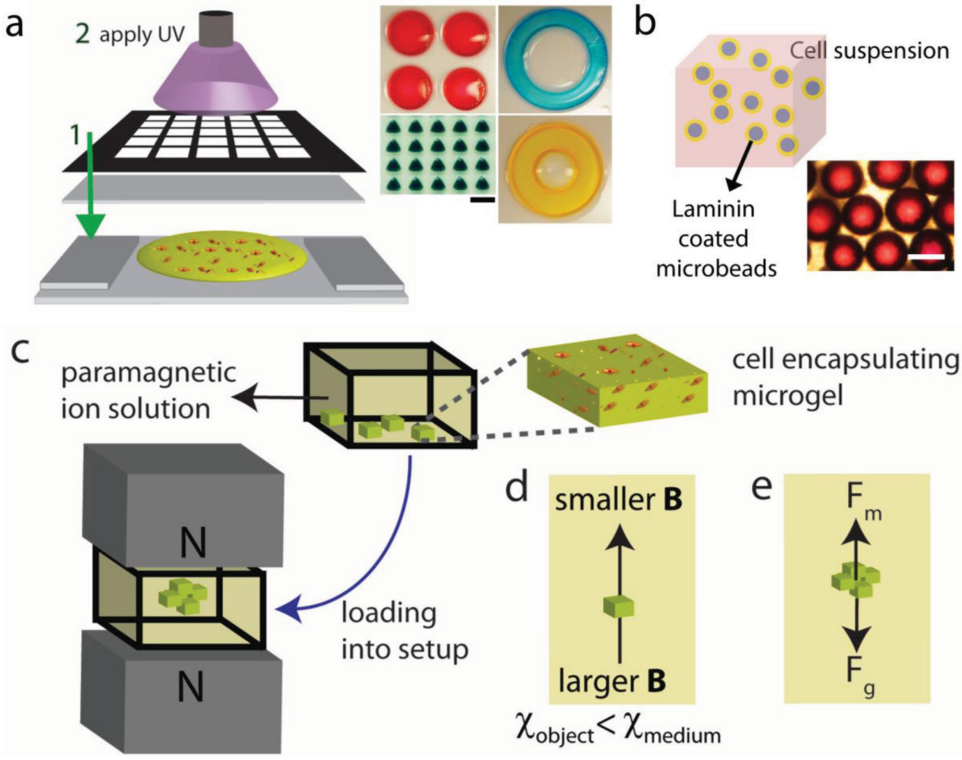


**Figure 1.** Levitational coding for soft living material fabrication. a) Schematic of hydrogel fabrication process. Hydrogel units were fabricated by photolithography with patterned masks at scales of many hundreds of micrometer. Gel precursor solution was pipetted onto a glass slide and then exposed to UV light. Scale bar is 1 mm. b) Cell seeded microbead fabrication. Images of microbeads coated with laminin first, and then incubated in cell suspension. Scale bar is 500 μm. c) Levitational self-assembly of cell-encapsulating building blocks in a mangetic setup composed of two NdFeB magnets with same poles facing each other. d) Object moves from larger magnetic field strength "B" to lower magnetic field strength, if the magnetic susceptibility of object is lower than magnetic susceptibility of the suspending medium. e) Forces acting on levitating objects at equilibrium height: magnetic force ($F_m$) and corrected gravitational force ($F_g$), which is the difference between gravitational force and buoyancy foce.

as cell encapsulating hydrogels or cell seeded microbeads in a paramagnetic suspending media for remote 2D and 3D manipulation and assembly. We demonstrated unique capabilities of this broadly applicable strategy in selective parallel assembly of polymers in the same reservoir and cell seeded beads for bottom-up tissue engineering and biofabrication.

The principles that underlie the fabrication and levitational assembly of soft living materials are summarized in **Figure 1**. Photo-crosslinkable polymers methacrylated gelatin (GelMA) or polyethylene glycol dimethacrylate (PEGDA) are used and crosslinked via UV light to fabricate microgels with patterned masks at scales of many hundreds of micrometers (Figure 1a). Cell seeded microbeads are also prepared and used as building blocks for assembly by first coating with laminin, and then incubating in cell suspension (Figure 1b). To paramagnetize suspension media, $Gd^{3+}$ ion salts have been used (Figure 1c). Cell-encapsulating hydrogels and cell seeded microbeads were randomly placed on the bottom surface of a reservoir filled with the paramagnetic medium. Upon placement of reservoir into magnetic setup composed of two permanent Neodymium (NdFeB) magnets with same poles facing each other, building units were assembled at the minimum magnetic field strength region due to magnetic susceptibility differences between building units and paramagnetic suspension media. In principle, object moves from a position with larger magnetic field strength to position with a lower magnetic field strength, if the magnetic susceptibility of object is lower than magnetic susceptibility of the suspending medium (Figure 1d). At the equilibrium height, buoyancy forces are balanced by the magnetic and gravitational forces (Figure 1e).

To characterize levitational soft material fabrication strategy, we first varied the number of PEG based hydrogels placed in $Gd^{3+}$ solution. Front view images of reservoirs placed into the magnetic setup are shown in **Figure 2**a. Each reservoir image shows different number of gels from $n$ = 2–50 at levitational equilibrium (from left to right, top to bottom). Here, we define assembly area as the front 2D area of the rectangle surrounding all of the gels. Assembly area linearly increased with the total number of gels assembled (assembly area = 0.54 × number of gels + 3.3, $R^2$ = 0.9945). Then, we kept the number of gels constant at 20, and obtained snapshots of the assembly reservoir over time (Supporting Information, Movie 1). Assembly area decreased as a function of time (Figure 2b). Then, we used microbeads and evaluated their assembly for a range of $Gd^{3+}$ concentrations: 0.1, 0.12, and 0.14 M. Results showed that based on the balance between magnetic force and counteracting corrected gravitational force, beads were assembled at different heights. On the other hand, their assembly area as a function of time showed a similar trend and all decreased to 5 (±0.72) $mm^2$ (Figure 2c).

To develop a better understanding of levitational assembly and its principles, we first demonstrated forces at equilibrium acting

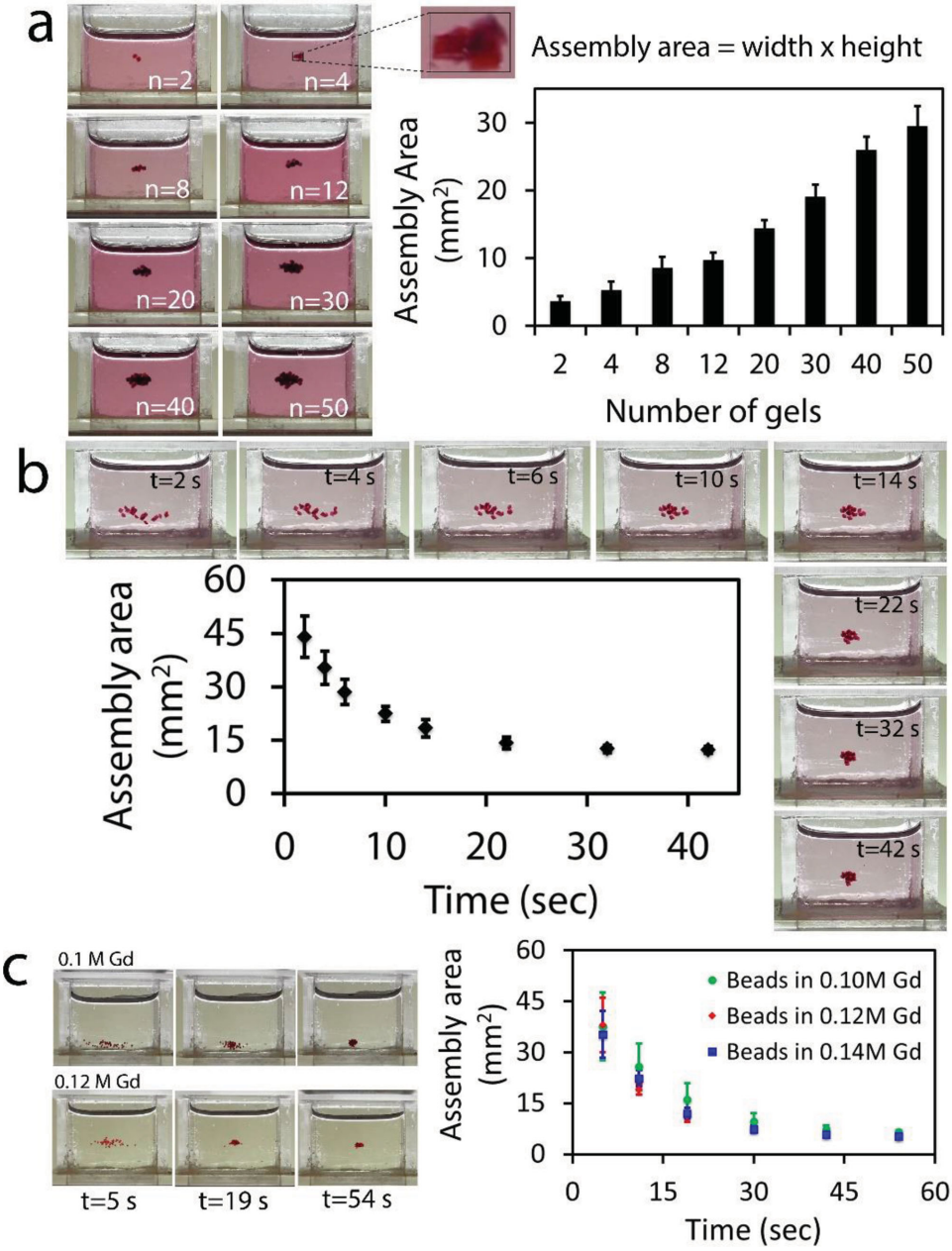


**Figure 2.** Characterization of levitational assembly. a) Front images of reservoirs placed into magnetic setup composed of two NdFeB magnets with same poles facing each other. Reservoirs include different numbers of gels from $n = 2$ to 50 (from left to right, top to bottom) at $t = 65$ s, when the hydrogels reach levitational equilibrium. Assembly area is defined as the area of the rectangle surrounding the gels. Assembly area linearly increases with the total number of gels. b) Assembly area of PEGDA gels (number of gels = 20) as a function of time (Supporting Information, Movie 1). Assembly area decreased as a function of time. c) Assembly area of microbeads as a function of time for a range of $Gd^{3+}$ concentration: 0.1, 0.12, and 0.14 M. Results showed that based on the balance between magnetic force and counteracting buoyancy force, beads were assembled at different vertical locations.

on a hydrogel or a microbead levitated in a paramagnetic medium (**Figure 3**a). Fluidic drag and inertial forces play a role, as well as magnetic and buoyancy forces during transient motion of hydrogel from bottom of the reservoir to the equilibration height. We simulated magnetic field norm (contour) and flux density (arrows) generated by two magnets with same poles facing each other (Figure 3b). Contour plot showed that magnetic minima formed at the central symmetry location of these two magnets. Then, we developed an analytical model of equilibration time as a function of equilibration height (Supporting Information, Equations (1)–(5)). We first plotted equilibration time of PEGDA gels as a function of equilibration height (Figure 3c), which matched with the experimental result of Figure 2b. By using the same analytical model,[18] we demonstrated equilibration time of microbeads as a function of equilibration height (Figure 3d,e). As shown in the insets, equilibration heights at (d) and (e) matched the experimental results of 0.1 and 0.12 M in Figure 2c, respectively. Agarose gels first levitated and self-assembled, and then sank due to absorption of paramagnetic

  

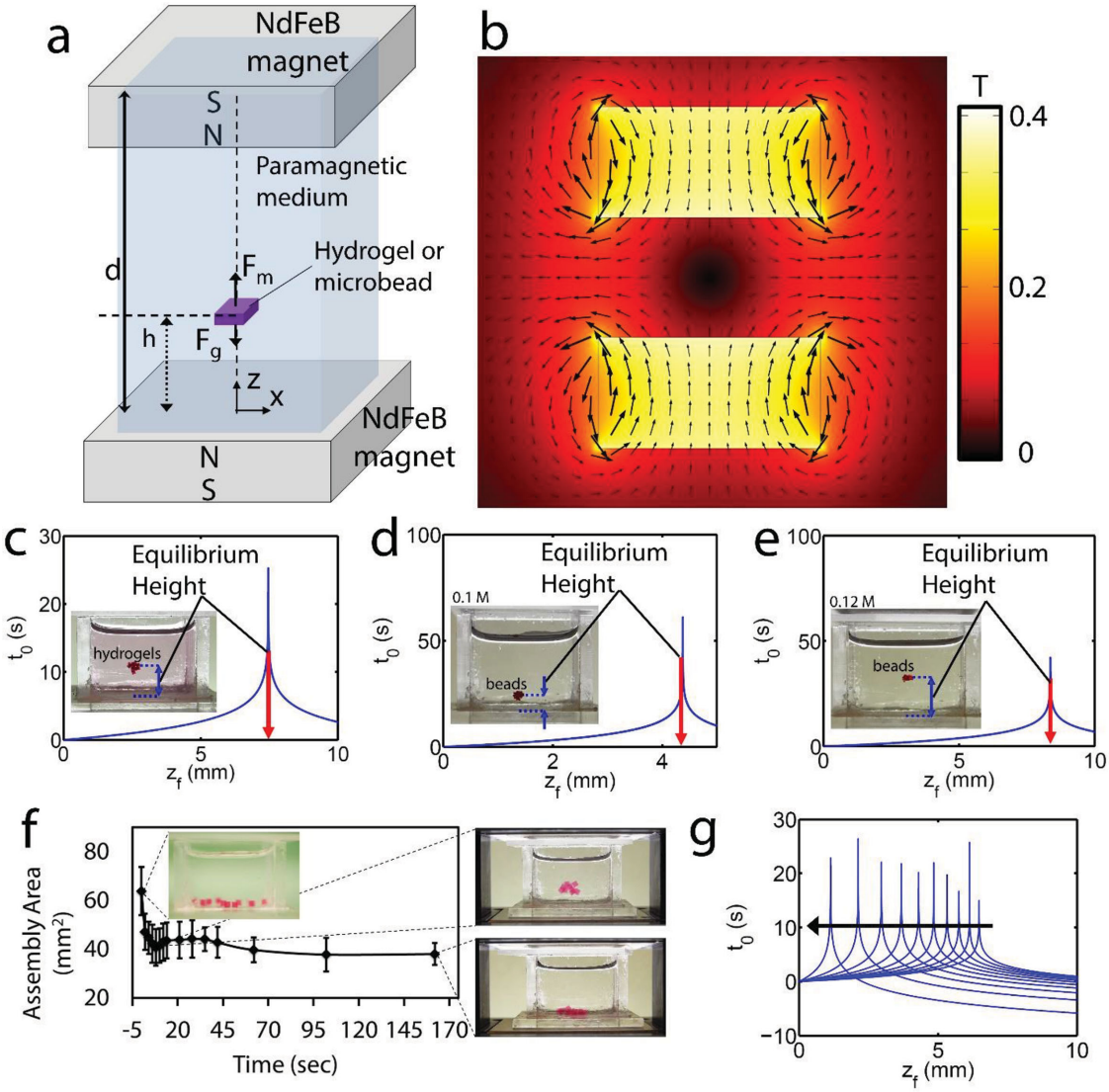


**Figure 3.** Underlying principles of levitational assembly. a) Illustration of forces at equilibrium acting on a hydrogel or a microbead levitated in a paramagnetic medium. During transient motion of hydrogel from bottom of the reservoir to the equilibration height, drag and inertial forces play a role as well as magnetic force ($F_m$) and buoyancy force ($F_b$). b) Simulation of magnetic field norm (contour) and flux density (arrows) created by two magnets with same poles facing each other. c) Analytical calculation of equilibration time (s) of PEG gels as a function of equilibration height. At the inset, equilibration height at c) matches with that of Figure 2b. d,e) Analytical calculation of equilibration time (s) of microbeads as a function of equilibration height. At the insets, equilibration heights at (d) and (e) match with that of 0.1 and 0.12 M in Figure 2c, respectively. f) Porosity and diffusion dependent magnetic signature change of gels, and dynamic levitation. We first quantified assembly area of agarose gels as a function of time (Supporting Information, Movie 2). Snapshots of assemblies at different time points. g) Then, we developed a mathematical model to include dynamic magnetic signature of objects to evaluate equilibration time and then sinking. Equilibration height declined while the susceptibility differences declined due to diffusion of paramagnetic medium into gels.

medium into gels (Figure 3f). Absorption dependent sinking did not disassemble the construct or disturb the assembled structure, as assembled gels stayed together. To account for porosity and diffusion dependent magnetic signature change of gels, and thus dynamic levitational equilibrium height, we extended the analytical model by including a diffusion dependent magnetic susceptibility coefficient (Supporting Information, Equations (1)–(5)). We first quantified assembly area of agarose gels as a function of time (Supporting Information, Movie 2). Then, we showed that equilibration height of gels approached zero as the magnetic susceptibility difference decreased (Figure 3g).

Following the characterization of self-assembly process, we studied patterning capability of levitational self-assembly strategy. We first fabricated two hollow-disk and a solid-disk PEG gels via UV lithography. Hydrogels were randomly placed at the bottom surface of the reservoir before being placed into the magnetic setup (**Figure 4**a,b). Upon placement of reservoir into the magnetic setup, gels were aligned horizontally at the center of magnets due to minimum magnetic field strength and equilibrated vertically at different heights due to differences in density among gel groups (Figure 4c and Supporting Information, Movie 3). To set a variety of mass densities among gels and tune their

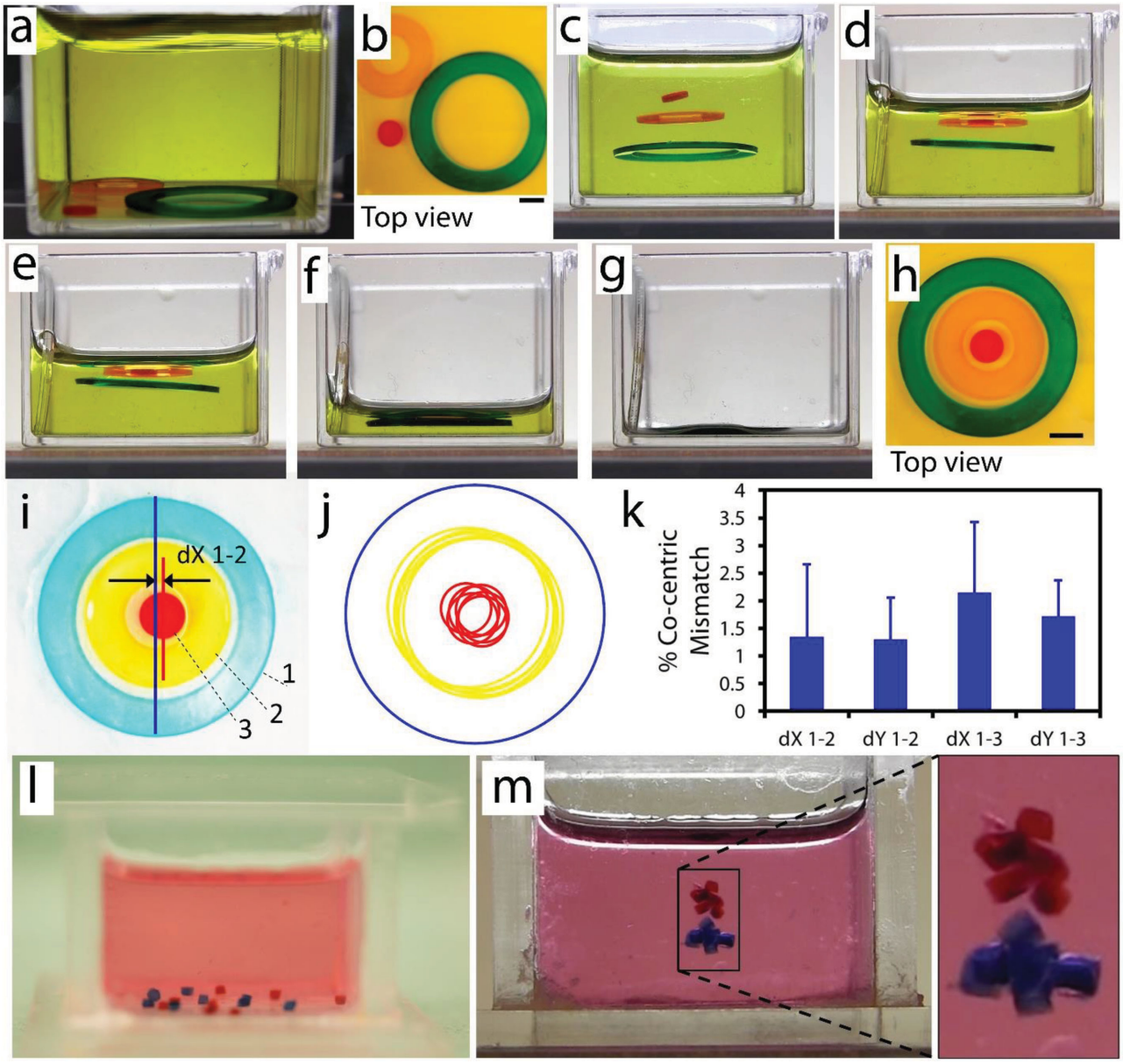


**Figure 4.** Levitational self-assembly of soft microcomponents. a–h) Concentric assembly of two hollow-disk and a solid-disk PEG gels (Supporting Information, Movie 3). a,b) Gels were randomly placed at the bottom of reservoir before being placed into a magnetic setup composed of two NdFeB magnets with like poles facing each other. c) Upon placement of reservoir into the magnetic setup, gels were aligned horizontally at the center of magnets due to minimum magnetic field strength and equilibrated vertically at different heights due to differences in densities among gel groups. Differences in gel densities were achieved by adding different amounts of polymer into precursor solution (red = 15% w/v, orange = 20% w/v, green = 50% w/v). d–g) Draining of the paramagnetic media from the reservoir decreased the height of air–liquid meniscus and caused a concentric deposition of gels. All scale bars are 1 mm. h) Final shape of assembled gels. i) Image of a concentric assembly with numerated gels. j) Mathematical equations of each circle were obtained by randomly picking three points at the outer circumferences of gels. Then, shapes were recreated using these mathematical equations, and plotted on top of each other while keeping the location of outer circle same. k) Concentric mismatches were calculated by finding the distances among centroids of two groups: 1–2) outer circle and middle gel, and 1–3) outer circle and inner gel. Results showed that concentric assembly has a high repeatability with around 2% mismatch ($n$ = 6). l,m) Selective levitational assembly of two types of PEG hydrogels (red = 20% w/v, blue = 50% w/v) (Supporting Information, Movie 4). l) Hydrogels at the bottom of the reservoir before being placed into the magnetic setup. m) Blue hydrogels and red hydrogels formed assemblies at different levels due to difference in their polymer concentration.

equilibration locations, different concentrations of PEGDA hydrogels (Red = 15% w/v, Orange = 20% w/v, Green = 50% w/v) were used in their respective precursor solutions. After alignment by magnetic forces, we drained the paramagnetic media out from the reservoir, which decreased the height of air–liquid meniscus and led to concentric stacking of gels (Figure 4d–g). Final shape of assembled gels is given in Figure 4h. Then, we quantified repeatability and precision of the self-assembly process. Here, we numerate concentric gels as 1–3 from outer to inner gel (Figure 4i). Mathematical equations of each circle were obtained

  

ADVANCED HEALTHCARE MATERIALS
www.advhealthmat.de

www.MaterialsViews.com

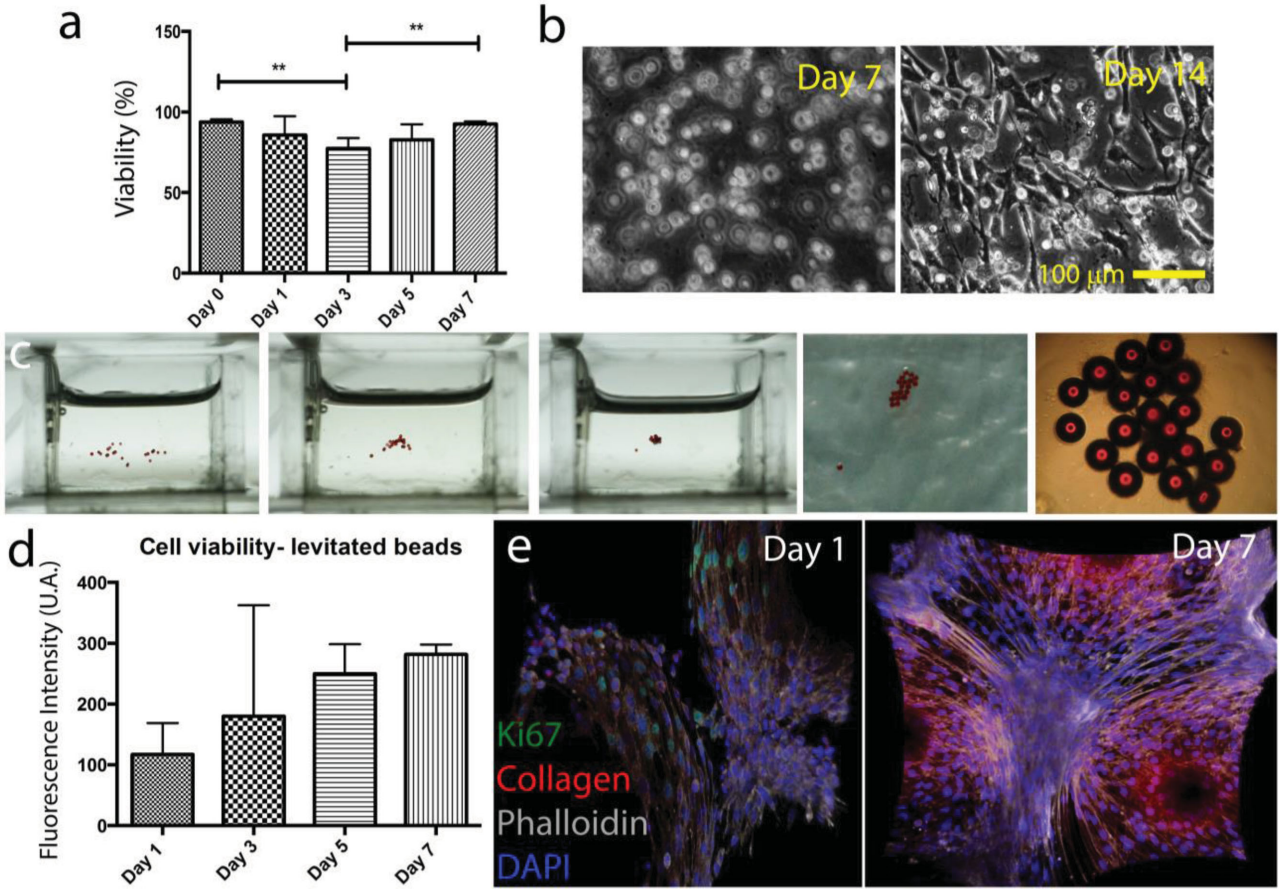


**Figure 5.** Evaluation of the effects of levitation and $Gd^{3+}$ medium on viability and proliferation. a) Long term viability results of $50 \times 10^{-3}$ M $Gd^{3+}$ treated hydrogel for 10 min. Lines connecting individual groups indicate statistically significant difference. One-way ANOVA with Tukey's post-hoc tests, $*p < 0.05$, $**p < 0.01$. b) Brightfield images of NIH3T3 mouse fibroblasts encapsulating 5 w/v% GelMA hydrogels after 7 and 14 d. c) 3T3 seeded microbeads were self-assembled in $50 \times 10^{-3}$ M $Gd^{3+}$ solution with magnetic levitation setup (total exposure time is 10 min). After levitational self-assembly and draining the suspension media out, beads were cross-linked with GelMA for stabilization. d) Cell viability results with Alamar Blue assay. Fluorescent intensity is given as a function of incubation days indicating the increase in biological activity, viability, and cell growth. e) Immunocytochemistry staining of cells seeded on assembled beads. Cell proliferation (ki67 green) and collagen secretion in a week after the levitation.

by randomly picking three points at the outer circumferences of gels via NIH ImageJ. Then, shapes were re-formed using these mathematical equations, and plotted on top of each other while keeping the location of outer circles same among all groups ($n = 6$) (Figure 4j). Next, concentric mismatches were calculated by evaluating the distances among centroids of two groups: (1–2) outer circle and middle gel, and (1–3) outer circle and inner gel. Results showed that concentric assembly has a high repeatability with approximately 2% mismatch (Figure 4k). After showing tunability of polymer concentration and equilibration height, we showed selective group assemblies of microgels. We fabricated two groups of PEGDA hydrogels (red = 20% w/v, blue = 50% w/v) (Figure 4l,m and Supporting Information, Movie 4). Hydrogels were again randomly placed at the bottom of the reservoir before being placed into the magnetic levitation setup (Figure 4l). 50% w/v PEG (blue) and 20% w/v PEG (red) hydrogels formed assemblies at different levels due to difference in their polymer concentration and resulting difference in gel densities (Figure 4m).

The patterning and assembly of cell-encapsulating/seeded microcomponents have several broad applications in numerous fields, including regenerative medicine, cell-based pharmaceutical research, and tissue engineering. The levitational assembly approach developed here offers a parallel precise patterning capability to create complex tissue microenvironments. To show this capability, we first evaluated the effects of levitation on the biological parameters such as cell viability, proliferation, and activity. NIH 3T3 mouse fibroblasts encapsulating 5 w/v% GelMA hydrogels were exposed to a range of $Gd^{3+}$ salt concentrations: $10 \times 10^{-3}$, $50 \times 10^{-3}$, and $100 \times 10^{-3}$ M, and then we performed live/dead assays. Immediately after the exposure to paramagnetic ion salts, live/dead results showed that for $10 \times 10^{-3}$ and $50 \times 10^{-3}$ M $Gd^{3+}$ concentrations, mean of cell viability rates are more than 90% (Supporting Information, Figure 3a). Next, we exposed hydrogels to only $50 \times 10^{-3}$ M $Gd^{3+}$ concentration for a range of exposure time: 5, 15, and 60 min. Immediately after the exposure for 5 and 15 min, viability results showed that the mean of cell viability rate is more than 70% (Supporting Information, Figure 3b). Then, to investigate long term viability, we exposed NIH3T3 mouse fibroblasts encapsulating 5 w/v% GelMA hydrogels to $50 \times 10^{-3}$ M $Gd^{3+}$ for 10 min, and then performed live/dead assay for days 0, 1, 3, 5, and 7 (**Figure 5**a). Here, we performed one-way ANOVA

with Tukey's post-hoc tests to find individual groups indicating statistically significant difference (*$p < 0.05$, **$p < 0.01$). Results showed that 3T3s are viable at day 7. Brightfield images of 3T3 encapsulating hydrogels at days 7 and 14 also showed that cells started to grow and synthesize extracellular matrix (ECM) at day 14 (Figure 5b). Then, we seeded 3T3s on laminin coated microbeads and assembled them via magnetic levitation in $50 \times 10^{-3}$ M $Gd^{3+}$ solution (Figure 5c). After levitational self-assembly and draining the suspension media out, beads were cross-linked with GelMA for stabilization. Cell viability results showed an increase in metabolic activity, viability, and cell proliferation over 7 days (Figure 5d). We also performed immunocytochemistry staining of cells at days 1 and 7, which indicated cell proliferation and ECM production in a week after the levitation (Figure 5e).

In summary, we have demonstrated a strategy for cell-encapsulating/seeded building units such as microgels or beads to be patterned in 3D and assembled in a contactless manner. Each building block can be easily programmed by composition, stiffness, elastic modulus, porosity, or cell type and then levitationally assembled with other building blocks into complex constructs with unique spatially heterogeneous material properties. We also showed selective levitational assembly of hydrogels by tuning their polymer concentration. A variety of 2D and 3D patterned assemblies can be fabricated by inexpensive permanent magnets without external power, and in an environment free of solid–solid contact. Our earlier work has shown use of radical paramagnetism in levitation of soft components.[13] However, their magnetic susceptibilities are orders of smaller than paramagnetic ion salts (Gd), which limits use of radicals in fast fabrication processes. Depending on the distance between magnets and the paramagnetic solution concentrations, we here show that millimeter-sized objects can be levitated and controlled precisely with this technique.[20]

The present strategy here can be a powerful yet simple biofabrication tool that enables several applications for bottom-up tissue engineering. Additionally, this strategy can be employed to generate more precise cell-free 3D hydrogel systems at relatively higher Gd concentration, as shown in Figure 4, to be used in soft robotics, or heterogeneous microphysiological system engineering for pharmaceutical research and diagnostics. After cell-free gel patterning is completed at relatively higher Gd concentration, ion salts can be washed away from gels, and cells can be seeded onto patterned hydrogels, e.g., for soft robotics. We envision that levitational assembly of soft living materials can be useful for inexpensive, parallel, contactless, and efficient manufacturing of biomaterials.

## Supporting Information

Supporting Information is available from the Wiley Online Library or from the author.

## Acknowledgements

U.D. acknowledges that this material is based in part upon work supported by the NSF CAREER Award Number 1150733, NIH R01EB015776-01A1, and NIH R21HL112114. U.D. is a founder of, and has an equity interest in, DxNow Inc., a company that develops microfluidic and imaging technologies for point-of-care diagnostic solutions. U.D.'s interests were reviewed and are managed by the Brigham and Women's Hospital and Partners HealthCare in accordance with their conflict of interest policies. S.T. acknowledges UCONN startup package and UCONN Research Excellence Award.

Received: February 9, 2015
Published online: April 14, 2015

[1] G. M. Whitesides, B. Grzybowski, *Science* **2002**, *295*, 2418.
[2] a) J. Yan, M. Bloom, S. C. Bae, E. Luijten, S. Granick, *Nature* **2012**, *491*, 578; b) J. Yan, K. Chaudhary, S. Chul Bae, J. A. Lewis, S. Granick, *Nat. Commun.* **2013**, *4*, 1516; c) K. Chaudhary, J. J. Juarez, Q. Chen, S. Granick, J. A. Lewis, *Soft Matter* **2014**, *10*, 1320.
[3] a) Y. Huang, X. Duan, Q. Wei, C. M. Lieber, *Science* **2001**, *291*, 630; b) W. Salalha, E. Zussman, *Phys. Fluids* **2005**, *17*, 063301; c) S. A. Stauth, B. A. Parviz, *Proc. Natl. Acad. Sci. U.S.A.* **2006**, *103*, 13922.
[4] D. Dendukuri, T. A. Hatton, P. S. Doyle, *Langmuir* **2006**, *23*, 4669.
[5] M. Tanase, D. M. Silevitch, A. Hultgren, L. A. Bauer, P. C. Searson, G. J. Meyer, D. H. Reich, *J. Appl. Phys.* **2002**, *91*, 8549.
[6] S. Tasoglu, D. Kavaz, U. A. Gurkan, S. Guven, P. Chen, R. Zheng, U. Demirci, *Adv. Mater.* **2013**, *25*, 1137.
[7] a) J. C. Hulteen, R. P. Van Duyne, *J. Vac. Sci. Technol. A* **1995**, *13*, 1553; b) A. D. Ormonde, E. C. M. Hicks, J. Castillo, R. P. Van Duyne, *Langmuir* **2004**, *20*, 6927.
[8] D. H. Gracias, J. Tien, T. L. Breen, C. Hsu, G. M. Whitesides, *Science* **2000**, *289*, 1170.
[9] a) K. L. Scott, T. Hirano, H. Yang, H. Singh, R. T. Howe, A. M. Niknejad, *J. Microelectromech. Syst.* **2004**, *13*, 300; b) U. Srinivasan, D. Liepmann, R. T. Howe, *J. Microelectromech. Syst.* **2001**, *10*, 17.
[10] a) Y. Lu, Y. Yin, Y. Xia, *Adv. Mater.* **2001**, *13*, 34; b) H. O. Jacobs, A. R. Tao, A. Schwartz, D. H. Gracias, G. M. Whitesides, *Science* **2002**, *296*, 323; c) Y. Xia, Y. Yin, Y. Lu, J. McLellan, *Adv. Funct. Mater.* **2003**, *13*, 907.
[11] a) S. E. Chung, W. Park, S. Shin, S. A. Lee, S. Kwon, *Nat. Mater.* **2008**, *7*, 581; b) S. E. Chung, Y. Jung, S. Kwon, *Small* **2011**, *7*, 796.
[12] F. Xu, C. A. M. Wu, V. Rengarajan, T. D. Finley, H. O. Keles, Y. R. Sung, B. Q. Li, U. A. Gurkan, U. Demirci, *Adv. Mater.* **2011**, *23*, 4254.
[13] S. Tasoglu, C. H. Yu, H. I. Gungordu, S. Guven, T. Vural, U. Demirci, *Nat. Commun.* **2014**, *5*, 4702.
[14] a) P. Chen, Z. Luo, S. Güven, S. Tasoglu, A. V. Ganesan, A. Weng, U. Demirci, *Adv. Mater.* **2014**, *26*, 5936; b) F. Xu, T. D. Finley, M. Turkaydin, Y. Sung, U. A. Gurkan, A. S. Yavuz, R. O. Guldiken, U. Demirci, *Biomaterials* **2011**, *32*, 7847.
[15] K. A. Mirica, F. Ilievski, A. K. Ellerbee, S. S. Shevkoplyas, G. M. Whitesides, *Adv. Mater.* **2011**, *23*, 4134.
[16] S. Wang, S. Tasoglu, P. Z. Chen, M. Chen, R. Akbas, S. Wach, C. I. Ozdemir, U. A. Gurkan, F. F. Giguel, D. R. Kuritzkes, U. Demirci, *Sci. Rep.* **2014**, *4*, 3796.
[17] K. A. Mirica, S. T. Phillips, C. R. Mace, G. M. Whitesides, *J. Agricultural Food Chem.* **2010**, *58*, 6565.
[18] K. A. Mirica, S. S. Shevkoplyas, S. T. Phillips, M. Gupta, G. M. Whitesides, *J. Am. Chem. Soc.* **2009**, *131*, 10049.
[19] N. D. Shapiro, K. A. Mirica, S. Soh, S. T. Phillips, O. Taran, C. R. Mace, S. S. Shevkoplyas, G. M. Whitesides, *J. Am. Chem. Soc.* **2012**, *134*, 5637.

  

[20] A. B. Subramaniam, D. Yang, H.-D. Yu, A. Nemiroski, S. Tricard, A. K. Ellerbee, S. Soh, G. M. Whitesides, *Proc. Natl. Acad. Sci. U.S.A.* **2014**, *111*, 12980.
[21] a) A. T. Skjeltorp, *J. Appl. Phys.* **1984**, *55*, 2587; b) A. T. Skjeltorp, *J. Appl. Phys.* **1985**, *57*, 3285.
[22] R. M. Erb, B. B. Yellen, *IEEE Trans. Magn.* **2006**, *42*, 3554.
[23] Y. Yang, L. Gao, G. P. Lopez, B. B. Yellen, *ACS Nano* **2013**, *7*, 2705.
[24] A. R. Kose, B. Fischer, L. Mao, H. Koser, *Proc. Natl. Acad. Sci. U.S.A.* **2009**, *106*, 21478.
[25] A. R. Kose, H. Koser, *Lab Chip* **2012**, *12*, 190.
[26] S. Tasoglu, J. Khoory, H. C. Tekin, C. Thomas, I. C. Ghiran, U. Demirci, *Adv. Mater.* **2015**, DOI: 10.1002/adma.201405660.